NIH Public Access
Author Manuscript
J Immunol. Author manuscript; available in PMC 2014 October 15.

Published in final edited form as:
J Immunol. 2013 October 15; 191(8): 4456–4465. doi:10.4049/jimmunol.1300827.

Identification of the cellular sentinels for native immunogenic Heat Shock Proteins *in vivo*

Michelle Nicole Messmer[1], **Joshua Pasmowitz**[1], **Laura Elizabeth Kropp**[2], **Simon C. Watkins**[3], and **Robert Julian Binder**[1,*]

[1]Department of Immunology, University of Pittsburgh, Pittsburgh, PA 15261

[2]Department of Microbiology and Immunology, Uniformed Services University of the Health Sciences Bethesda, MD 20814

[3]Department of cell Biology, University of Pittsburgh, Pittsburgh, PA 15261

Abstract

Select members of the heat shock proteins (HSPs) family, such as gp96, elicit immune responses specific to their chaperoned peptides. While immunological effects of HSPs on antigen presenting cell (APCs) described to date have largely been demonstrated with cell lines or primary cells in culture, their collective responses *in vitro* have been consistent with priming immune responses. Here we examine the physiologically relevant APCs in mice that are targeted following vaccination with native, murine HSP and characterize those cells. Gp96 accesses the subcapsular region of the draining lymph node and is internalized predominantly by $CD11b^+$ cells in this locale. Cells acquiring gp96 can transfer protective anti-tumor immunity to naïve mice by actively cross-presenting gp96-chaperoned peptides and providing co-stimulation. Our studies illustrate how HSPs act to alert the immune system of cellular damage and will be of paramount importance in immunotherapy of patients with cancer and infectious disease.

Keywords

gp96; CD91/LRP1; dendritic cell; antigen presenting cell

Introduction

The immunogenic HSPs elicit immune responses that are specific for the peptides that they chaperone (1). Hence HSPs purified from tumor cells or cells infected with pathogens are able to elicit protective and therapeutic immunity in mice and humans vaccinated with such preparations (2–7). These immunogenic HSPs include gp96 (2,4,5), hsp70 (5,8,9), hsp90 (9), calreticulin (10), hsp110 (11) and grp170 (11). The immunogenicity of these HSPs is attributed to their remarkable ability to bind to the receptor CD91 present on antigen presenting cells (12–13). Interaction of HSPs with CD91 allows the engaging APC to cross-present antigens that are chaperoned by HSPs (2,12). Internalized HSP-peptide complexes are processed by APC before presentation of peptides by MHC I and II (13–14). CD91 increases the efficiency of cross-presentation when compared to non-CD91 mediated uptake of soluble antigens. This allows for priming of immune responses even when antigen loads are low. In addition, HSPs signal through CD91 via phosphorylation of the cytosolic domains of the receptor (15). The signals trigger activation of NF-κB and p38 MAPK. The

*To whom correspondence should be sent: Robert J. Binder, Ph.D., University of Pittsburgh School of Medicine, E1051 Biomedical Science Tower, 200 Lothrop Street, University of Pittsburgh, Pittsburgh, PA 15261, tel: 412-383-7722, fax: 412-383-8098.

NIH-PA Author Manuscript
NIH-PA Author Manuscript
NIH-PA Author Manuscript

NIH-PA Author Manuscript

NIH-PA Author Manuscript

NIH-PA Author Manuscript

net result is maturation of APCs with simultaneous release of numerous cytokines and up-regulation of expression of co-stimulatory molecules (15,16). These two events are necessary for priming robust T cell responses. Subsequently we have shown that release of HSPs from aberrant cells such as tumors is necessary for priming concomitant immunity (17).

Studies detailing the immunological effects of HSPs have used myriad APCs *in vitro*, ranging from bone marrow derived cells cultured in GMCSF with or without IL-4 (16), peritoneal exudates containing macrophages (16), B cells (18), and macrophage- and dendritic-like cell lines (19). Expectedly, the different types of APCs produced a diversity of responses, in cytokine production and cross-presentation. What then are the physiologically relevant APCs necessary for the immunological responses elicited by vaccination with HSPs? One experiment performed almost 2 decades ago tested the requirement for APCs during HSP immunization by using the broadly acting reagent carrageenan, which inhibits the function of all phagocytic cells; T cell priming was abrogated in those studies (20). One decade ago we showed that $CD11c^{+}$ cells from lymph nodes of gp96-immunized mice could transfer tumor immunity, but the phenotype of these cells and whether they endocytosed gp96 was not further characterized (21). More recently, the efficiency of priming anti-tumor immune responses with a genetically engineered and secreted form of gp96 (gp96-Ig) was explored. Those studies showed that intraperitoneal vaccination with these fusion proteins caused a dramatic increase of $CD11c^{high}MHCII^{high}CD103^{+}$ cells in the peritoneum (22). While these APCs were able to induce the expression of gut-homing receptor CCR9 in responding T cells *in vitro*, their requirement *in vivo* was not tested (22). Our understanding of APC subset dynamics with regards to intradermal vaccination with native, murine gp96 and CD91 expression remains unexplored and warrants an investigation. A compilation of APC subsets and their functional relevance to priming adaptive immunity has been reviewed elsewhere (23–24). These studies will have an impact on clinical trials as the route of HSP administration remains routinely intradermal/subcutaneous.

Following introduction of extracellular gp96 in mice via immunization, gp96 was shown to preferentially localize to cells with CD11b and CD11c. Subsets of APCs are further characterized with respect to CD4, CD8, Gr1.1, MHC II, F4/80, CD103 and CD207 expression. Anti-tumor immunity could be transferred to naïve mice by adoptive transfer of cells that were positive for gp96 acquisition. While CD91 expression is essential for gp96 uptake, location of APCs within the lymph node was another determining factor for acquiring HSP. These results are extrapolated to HSPs in the extracellular environment following active release by, or necrotic death of, aberrant cells. This study is important for development of novel HSP-based vaccines for immunotherapy of cancer and infectious disease and in improvement of on-going clinical trials. Finally, these studies will shed light on the observations that HSPs are capable of priming Th1 (2,4,5,20,22), Th2 (25,26), Th17 (15) and Treg (27–28) responses under different immunization conditions.

Methods

Mice

C57BL/6, BALB/c and C57BL/6 x BALB/c F1 mice were purchased from The Jackson Laboratory (Bar Harbor, ME). Experimental mice were used between the ages of six to eight weeks. All mice were used according to IACUC protocols approved by the University of Pittsburgh and in accordance with the National Institutes of Health (Bethesda, MD) guidelines.

NIH-PA Author Manuscript

NIH-PA Author Manuscript

NIH-PA Author Manuscript

Cells and reagents

CMS5 and RAW264.7 cells were obtained from ATCC (Manassas, VA). BMDCs were obtained by culturing bone marrow cells for 6 days in GMCSF. Apparently homogenous preparations of gp96 were labeled with Alexafluor 488 (Invitrogen, Grand Island, NY) exactly as recommended to obtain $gp96_{A488}$. Each molecule of gp96 was calculated to be labeled with 4–9 molecules of A488. Protein was analyzed by standard SDS-PAGE and immunoblotting with anti-gp96 (Enzo Life Sciences, Inc. Farmingdale, NY) and anti-A488 (Invitrogen, Grand Island, NY) antibodies. For the CMS5 tumor experiment, ERK peptide (QYIHSANVL) was conjugated to $gp96_{A488}$ as previously described (29), termed $gp96_{A488}$-ERK. Free peptide was removed by size exclusion membranes. HELOVA peptide consists of the HEL14 peptide ($HEL_{12–15}$) in tandem with the OVA8 peptide ($OVA_{257–264}$). The ovalbumin protein (OVA) and hen egg lysozyme protein (HEL) were purchased from SIGMA (St. Louis, MO). All peptides were synthesized at Genemed Synthesis, Inc. (San Antonio, TX). Gp96-HELOVA complexes were made as above. For tracking peptides within BMDCs, an OVA20 mer peptide was biotinylated and then complexed to $gp96_{A488}$ to obtain $gp96_{A488}$-b-pep20.

Tracking gp96 *in vivo*

Mice received ventral intradermal immunizations with $gp96_{A488}$ in 100 μl saline. Doses of $gp96_{A488}$ are indicated in each experiment. In some experiments, lymph nodes were isolated after indicated incubation periods, mechanically disrupted and passed through a 20μm strainer.

Flow cytometry

Cells were blocked with anti-CD16/CD32 antibody (BD Pharmingen, San Diego, CA) for 10 minutes before addition of fluorescent-tagged surface antibodies for 20 minutes. Where indicated, cells were fixed in 4% paraformaldehyde and stained with CD91 antibody 5A6 (Abcam, Cambridge MA) followed by FITC conjugated rat anti-mouse IgG2b (BD Pharmingen). The following antibodies were used: CD11c allophycocyanin, CD11b PECy7, CD8 Pacific Blue, CD4 PerCPCy5.5, CD207 PE, MHC class II PE (rat anti-mouse I-A/I-E), CD103 PE, Gr1.1 PerCPCy5.5, and F4/80 Brilliant Violet 450 (BD Pharmingen). Data was collected on a Becton Dickinson LSR2 (Franklin Lakes, NJ) using Cellquest software and analyzed using FlowJo version 7 (Treestar, Inc., Ashland, OR). The negative thresholds were set by comparing unstained controls with single color controls for each fluorophore and taking into account any overlap from additional dyes used.

Adoptive transfer of cells

Lymph node cells were harvested from BALB/c mice 6 hours after vaccination with $gp96_{A488}$ or $gp96_{A488}$-ERK and sorted by FACSAria (BD Bioscience, San Jose CA) based on A488 positivity. 1×10^5 sorted cells were transferred to naïve BALB/c mice retro-orbitally. Mice were challenged intradermally one week later in the dorsum with 1×10^6 CMS5 cells. Tumor growth was monitored.

Microscopy

Lymph nodes were fixed in 2% paraformaldehyde and then stored in 30% sucrose solution at 4°C overnight. Tissues were frozen by submersion in 2-methyl-butane cooled by liquid nitrogen and stored long term at −80°C. Sections (8–10 μm) were prepared in Neg50 freezing media on a HM505 Microm Cyrostat, and adhered to Fisherbrand Superfrost Plus Precleaned Microscope Slides (Fisher Scientific). Slides were stored at −20°C until staining (CBI, University of Pittsburgh). Primary antibodies included biotin conjugated CD11b, CD4, CD8, CD207, CD103 and purified Armenian Hamster anti-CD11c (BD Pharmingen &

NIH-PA Author Manuscript

NIH-PA Author Manuscript

NIH-PA Author Manuscript

eBioscience, San Diego, CA). Secondary antibodies were Cy5-goat-anti-Hamster IgG and DyLight 549-Streptavidin (Jackson ImmunoResearch, West Grove, PA). To visualize intracellular trafficking of gp96-peptide complexes, BMDCs were grown overnight on coverslips. $Gp96_{A488}$-b-pep20 was pulsed onto BMDCs for indicated times at 37°C or 4°C. Cells were washed, fixed and permeabilized. Cells were stained with Cy3-strepavidin (Jackson ImmunoResearch), phalloidin and/or LAMP-1 specific antibody (Invitrogen). All images were captured using an Olympus 1000 inverted confocal microscope with 60x objective and Fluoview v. 2.1 acquisition software (Melville, NY). Imaris v. 7.2.1 (Bitplane, Zürich, Switzerland) and Photoshop v. 7.0 (Adobe, San Jose, CA) were used for analysis and to prepare the images for publication.

Analysis of CD91 expression

Lymph node cells were sorted by FACSAria based on staining with CD11c allophycocyanin and CD11b PECy7 antibodies (BD Pharmingen). Cells were washed and 30–50,000 cells from each subset were lysed in SDS containing sample buffer and analyzed by standard PAGE. Immunoblotting was performed using the monoclonal rabbit anti-CD91 antibody EPR3724 (Abcam). Equivalent cell numbers of RAW264.7 and EL.4 were loaded as positive and negative controls, respectively.

Cross-presentation assay

In separate duplicate wells, BMDCs were cultured in 200 μl of complete media containing 20 μg of gp96-HELOVA, HEL or OVA, or 0.05 μg HELOVA, 0.03 μg HEL14 or 0.17 μg OVA8. T cell hybridomas B3Z specific for OVA8/K^b (30) or LC21 specific for HEL14/IA^d (31) were added at BMDC to T cell hybridoma ratio of 1:1 with 1×10^5 cells of each. B3Z was developed as previously described (30) and IL-2 was measured by ELISA for LC21 activation.

Statistical Analysis

Differences between the means of experimental groups were analyzed using the two tailed Student's *t*-test. Differences were considered significant when $p \leq 0.05$.

Results

Rapid draining of gp96 to lymph nodes

Apparently homogenous preparations of gp96 were labeled with Alexafluor 488 ($_{A488}$). We confirmed labeling by SDS-PAGE and immunoblotting (Supplemental Figure 1A). Alexafluor 488-labeled gp96 ($gp96_{A488}$) remained functional as determined by binding and uptake by the CD91-expressing, macrophage cell line RAW264.7. RAW264.7 cells incubated with $gp96_{A488}$ endocytosed significant amount of the protein as measured by flow cytometry (Supplemental Figure 1B) and microscopy (Supplemental Figure 1C). Gp96, labeled on primary amines in a similar manner, has previously been shown to retain its immunological property of priming T cell responses (32). Mice were then immunized intradermally with titrated doses of $gp96_{A488}$. A dose of 1–10 μg administered via this route has routinely been used to elicit tumor-specific T cell responses (2,4,5,20,27). Single cell suspensions of draining axillary and inguinal lymph nodes were analyzed by flow cytometry 8 hours post immunization (Supplemental Figure 2A). Significant A488 signal was detected in the lymph nodes at ≥10 μg dose when compared to lymph nodes from mice immunized with PBS (Figure 1A). We performed a kinetic experiment by immunizing sets of mice with 10μg $gp96_{A488}$ and harvesting draining lymph nodes from mice at the indicated time points (Supplemental Figure 2B). Gp96 was observed in the lymph node as early as 1 hour following immunization and peaked at that point (Figure 1B). The signal gradually

NIH-PA Author Manuscript

NIH-PA Author Manuscript

NIH-PA Author Manuscript

decreased thereafter but was still detectable 72 hours post immunization. In addition, we visualized the interaction of $gp96_{A488}$ with lymph node cells by fluorescent microscopy (Figure 1C). Two populations of cells, differing in the amount of $gp96_{A488}$ internalized, could be discerned. These results demonstrate that gp96 can be rapidly detected in lymph node cells following intradermal immunization and suggests differential uptake by cell populations.

Acquisition of gp96 by $CD11b^+$ and $CD11c^+$ cells

We began a systematic analysis of lymph nodes by a broad screen based on the surface markers CD11c and CD11b which are associated with professional cross-presenting APCs. The gating strategies are outlined in Supplemental Figure 3. The total lymph node was observed to have ~2% and ~10% of $CD11c^+$ and $CD11b^+$ cells respectively (Figure 2A). These subsets can be further divided on additional APC markers including MHC II, CD4, CD8, F4/80, Gr1.1, CD103 and CD207 as shown in Supplemental Figure 3D–G. This analysis was applied to draining lymph nodes harvested from mice immunized with 10 μg of $gp96_{A488}$. $A488^+$ cells in the draining lymph node were harvested at 8 or 48 hours after immunization. At 8 hrs, $CD11b^+$ cells ($CD11c^{+/-}$) comprised ~70% of the $gp96_{A488}{}^+$ cells at the 8 hour time point (Figure 2A). These $gp96^+$ cells expressing CD11b were additionally phenotyped for CD4, CD8, Gr1.1, F4/80, and MHC II (Figure 2B, Supplementary Figure 3D–F). $CD11b^+gp96^+$ cells were primarily $CD4^+$, $CD8^-$, $Gr1.1^-$ with low or no F4/80 expression and abundant MHC II expression (Figure 2B). About 30% of $gp96_{A488}{}^+$ cells in the lymph node were $CD11c^+$ ($CD11b^{+/-}$) at 8hrs (Figure 2A). These cells were further phenotyped for CD4, CD8, CD207, CD103, and MHC II (Supplemental Figure 3D, E, G). $CD11c^+gp96^+$ cells also had abundant MHC II expression, however the expression of CD103 and CD207 was heterogeneous (Figure 2C). A greater percentage of the cells had no CD207 or CD103 expression. Cells that were $CD11b^-CD11c^-$, primarily B and T cells and comprising a bulk (~93%) of the lymph node, accounted for the remaining 30% of $gp96_{A488}{}^+$ cells (Supplemental Figure 3C).

We next compared the overall distribution of cell types with $gp96_{A488}$ at 8hrs. A significantly greater percentage of $CD11b^+CD4^+$ cells acquired $gp96_{A488}$ compared to $CD11b^+CD4^-$ cells (Figure 2D, Supplemental Figure 3E). $CD11c^+$ cells were a smaller fraction of $gp96^+$ cells and included both $CD8^+$ and $CD8^-$ cells, though $CD8^-$ cells were the major $CD11c^+$ fraction. (Figure 2D). At 48 hrs post immunization the distribution of $gp96_{A488}$ was essentially the same (Figure 2D, E); $CD11b^+$ cells were still the larger percentage of $gp96_{A488}$ compared to $CD11c^+$ cells. However the percentage of $CD11c^+CD8^+$ cells doubled in $gp96_{A488}$ positivity at 48 hrs compared to the 8 hour time point. These data characterize the distribution of gp96 in draining lymph nodes following immunization at early and late time points.

Gp96 is localized to cells of the subcapsular region of the draining lymph nodes

We used fluorescent microscopy to obtain a panorama of the draining lymph node following immunization with $gp96_{A488}$. Mice were immunized with 10 μg $gp96_{A488}$ and sequential tissue sections were prepared 8 hours post injection. As shown in Figure 3A, $gp96_{A488}$ localizes to the subcapsular region of the lymph node. This region of the lymph node is populated primarily by $CD11b^+$ cells as shown in the highlighted region of interest (Figure 3B) and is distinct from the T cell zones as shown by co-staining for CD8 (Figure 3C). The overlap of $gp96_{A488}$ signal with CD11b and/or CD11c was quantified using IMARIS software and substantiates the results obtained by flow cytometry in Figure 2; early after immunization (8hrs) $gp96_{A488}$ is associated more with $CD11b^+$ than $CD11c^+$ cells (Figure 3D). Draining lymph node sections from mice immunized with $gp96_{A488}$ were stained for CD207 (Langerin) at the 8 hour time point (Figure 3E). A small fraction of $gp96_{A488}$

NIH-PA Author Manuscript

NIH-PA Author Manuscript

NIH-PA Author Manuscript

colocalized to CD207 consistent with observations in Figure 2C. We next examined the overlap of $gp96_{A488}$ with CD103, an integrin that identifies a subset of lymph node dendritic cells. We observed some co-localization of $gp96_{A488}$ with CD103 although this association was variable (Figure 3D, F, G). These data are consistent with the flow cytometry data in Figure 2. At 8 hrs following immunization, $gp96_{A488}$ is taken up by primarily by $CD11b^+$ ($CD11c^{+/-}$) cells in the subcapsular region of the lymph node.

Functional $gp96^+$ APCs transfer tumor-specific immunity

As shown in previous studies conducted *in vitro*, gp96 stimulates APCs rendering them capable of providing signals for priming T cells. In addition, peptides (including tumor antigens) chaperoned by gp96 are cross-presented by the same APCs. We set up an antigenic system based on the CMS5 tumor and its immuno-dominant peptide ERK (33), to test whether the APCs that captured gp96 *in vivo* were immunogenic (Figure 4A). $Gp96_{A488}$ was complexed to the ERK peptide ($gp96_{A488}$-ERK) or left uncomplexed ($gp96_{A488}$). Mice were immunized with 10μg of $gp96_{A488}$-ERK, $gp96_{A488}$, ERK or PBS. $A488^+$ cells were isolated from draining lymph nodes from each group of mice after 6 hours by FACS (Figure 4B). $A488^+$ cells from $gp96_{A488}$-ERK or from $gp96_{A488}$ group, or bulk lymph node cells from ERK peptide or PBS immunized group, were transferred to naïve BALB/c mice retro-orbitally. Recipient mice were challenged one week later with CMS5 cells (Figure 4A). Tumor growth rate was measured. Tumor growth was significantly retarded only in mice that received $A488^+$ cells from donors immunized with $gp96_{A488}$-ERK. Tumors grew with identical kinetics in mice receiving $A488^+$ cells from donors immunized with $gp96_{A488}$, or mice receiving bulk lymph node cells from donors immunized with ERK peptide or PBS (Figure 4C). We tested whether the protective effect was dependent on the cross-priming ability of donor ($A488^+$cells) or recipient APCs. Cells from donors, immunized with $gp96_{A488}$-ERK or $gp96_{A488,}$ were irradiated prior to adoptive transfer to recipient naïve mice as above. Recipients were then challenged with CMS5. Tumor growth rate was measured (Figure 4D). The protective effect of $A488^+$ cells from $gp96_{A488}$-ERK immunized mice was abrogated when they were irradiated, as the tumors grew with identical kinetics to control treated or untreated mice. This demonstrates that the transferred (donor) APCs were actively involved in priming anti-tumor immunity through events that may include antigen transfer, cross-presentation and migration.

Differential expression of CD91 in APC subsets

We have previously shown that CD91 expression is essential for gp96 uptake. Thus we tested the relative expression of CD91 by APCs in the lymph node as characterized by their expression of CD11b and/or CD11c (Figure 5A). Cells were stained for CD91 simultaneously with CD11b and CD11c and analyzed by flow cytometry. CD91 expression was observed to vary with each population (Figure 5B, Supplemental Figure 4A). $CD11c^+CD11b^+$ cells had the most robust CD91 expression as measured by geometric MFI followed by $CD11c^-CD11b^+$ cells. CD91 expression on $CD11c^+CD11b^-$ cells, while barely detectable, was still significant over background staining with secondary antibody alone. CD91 expression was not significantly detected on $CD11c^-CD11b^-$ cells in this assay although this observation does not conflict with the possibility that a minor cell type in this large and varied population does so (34,35). The results in Figure 5B were confirmed by immunoblotting. FACS purified APC populations from the lymph node were lysed and analyzed by SDS-PAGE and immunoblotted for the β-chain of CD91 (85kDa). CD91 expression was easily detectable in the $CD11c^+CD11b^+$ population and, at equivalent cell numbers, more difficult to discern in $CD11c^-CD11b^+$ and $CD11c^+CD11b^-$ populations (Figure 5C). The macrophage cell line RAW264.7 served as a positive control and EL.4 thymoma as the negative control cells for CD91 expression.

NIH-PA Author Manuscript

NIH-PA Author Manuscript

NIH-PA Author Manuscript

CD91 expression correlates with superior gp96 endocytic capacity

We tested the ability of various lymph node APCs to endocytose gp96 *in vitro*. We exposed total lymph node cells directly to sub-saturating levels of $gp96_{A488}$ *in vitro* and analyzed them by flow cytometry (Figure 6). Consistent with the data in Figure 1A, the percent of $gp96_{A488}^{+}$ cells was titratable with increasing amounts of $gp96_{A488}$ (Figure 6A). Lymph node cells were phenotyped for CD11b and CD11c expression (Figure 6B). Regardless of the amount of $gp96_{A488}$ provided to lymph node cells, $CD11b^{+}CD11c^{+}$ cells endocytosed the most $gp96_{A488}$ as measured by geometric mean fluorescence intensity (Figure 6C); cells expressing the highest levels of CD91 (Figure 5). As a population, $CD11c^{-}CD11b^{-}$ cells appeared to acquire very little $gp96_{A488}$ (Figure 6C) correlating with their lack of CD91 expression. $CD11c^{+}CD11b^{+}$ cells, representing lymph node resident APCs, acquired the most $gp96_{A488}$ as a population although they represented a small proportion of cells in the lymph node. This result was the same across a wide range of $gp96_{A488}$ sub-saturating concentrations. In addition, incubations of cells with $gp96_{A488}$ for different lengths of time did not change the outcome; significantly more $gp96_{A488}$ was associated with $CD11c^{+}CD11b^{+}$ cells than other cells at all time points measured (Figure 6D).

We next investigated the level of efficiency of $gp96_{A488}$ incorporation in competition studies by removing $CD11c^{-}CD11b^{-}$ cells and performing the same experiment with purified populations of isolated $CD11b^{+}$ and $CD11c^{+}$ cells and sub-saturating concentrations of $gp96_{A488}$. Lymph node cells were sorted into $CD11c^{+}CD11b^{-}$ or $CD11c^{+}CD11b^{+}$ populations. These two populations of cells were mixed in comparable numbers (Figure 6E) and incubated with $gp96_{A488}$. Cells were analyzed by flow cytometry for their level of $gp96_{A488}$ incorporation (Figure 6F). $CD11c^{+}CD11b^{+}$ cells were observed to incorporate significantly more $gp96_{A488}$ than $CD11c^{+}CD11b^{-}$ cells. A similar experiment was performed with isolated $CD11c^{+}CD11b^{+}$ cells mixed with $CD11b^{+}CD11c^{-}$ cells (Figure 6G). $CD11c^{+}CD11b^{+}$ cells were again observed to incorporate significantly more $gp96_{A488}$ than $CD11b^{+}CD11c^{-}$ cells (Figure 6H). The acquisition of $gp96_{A488}$ by $CD11c^{+}CD11b^{+}$ cells was unaffected by the presence (mixed) or absence (unmixed) of other $CD91^{+}$ ($CD11b^{+}CD11c^{-}$) cells (Figure 6I). We thus conclude that $CD11c^{+}CD11b^{+}$ APCs, characterized by robust CD91 expression, appear superior at endocytosis of gp96 compared to other lymph node cells with lesser or no CD91 expression.

Peptides chaperoned by HSPs are cross-presented by $CD11b^{+}CD11c^{+}$ cells

Cross-presentation of HSP-chaperoned peptides after uptake by CD91 is necessary for priming effective immune responses (Figure 4) (2,12). To study the cross-presentation of peptides chaperoned by HSPs, significantly more $CD11b^{+}CD11c^{+}$ cells were required for the experiments below than could be obtained from lymph nodes. Therefore we used bone marrow derived dendritic cells (BMDCs) which express a similar phenotype including $CD11c^{+}CD11b^{+}$ markers (36) as the cells we examined in Figure 6, in addition to CD91 (13). We first confirmed that the BMDCs were functionally competent in cross-presenting gp96-chaperoned peptides on either MHC I or MHC II molecules. Gp96, complexed to a 22-mer peptide (HELOVA) consisting of HEL 14-mer peptide presented by H-$2IA^{d}$, in tandem with the OVA8-mer peptide presented by H-$2K^{b}$. The gp96-HELOVA complex was incubated with BMDCs from H-2^{b} (C57BL/6) x H-2^{d} (BALB/c) F1 BMDCs under conditions previously shown to allow for cross-presentation of the chaperoned peptides. Briefly BMDCs were incubated with 10 μg of gp96-peptide complexes and T cell hybridomas specific for OVA8/K^{b} (B3Z) or HEL14/IA^{d} (LC21). Peptides chaperoned by gp96 were cross-presented by F1 BMDCs and were detected by B3Z (Figure 7A) and LC21 (Figure 7B) respectively. HELOVA peptide alone at a concentration similar to what was introduced to the assay in a complex with gp96, was poorly cross-presented. Similarly, as we have previously shown, whole protein (OVA or HEL) was poorly cross-presented.

NIH-PA Author Manuscript

NIH-PA Author Manuscript

NIH-PA Author Manuscript

Endosomal localization of gp96 within APCs following uptake has previously been visualized (37). Therefore we further examined trafficking of HSP *and* chaperoned peptides within cells. Here, $gp96_{A488}$ was complexed to a biotinylated 20mer peptide (b-pep20). Cells were incubated with 10 μg of $gp96_{A488}$-b-pep20 for the indicated times points and temperatures (Figure 7C–F). Cells were fixed, permeabilized and stained with streptavidin-Cy3 (for detection of peptide) and phalloidin for detection of actin filaments. Co-localization was quantified using the IMARIS software to obtain the Pearson's coefficient of colocalized volume (Figure 7G–I). At 5 minutes most of the peptide was bound to gp96, but the two molecules appeared to be dissociated by 15 minutes (Figure 7C, D, G). At 15 minutes peptide was co-localized with actin, suggesting translocation into the cytosol (Figure 7D, H). Surprisingly, gp96 also co-localized with actin, (Figure 7I). This detection was rapid and occurred within 5mins, suggesting that, first, gp96 translocated to the cytosol independently of peptide and, second, gp96 dissociated from the peptide in the endosome prior to translocation. BMDCs incubated with $gp96_{A488}$-b-pep20 were stained with LAMP-1, a lysosomal marker (Figure 7J). Gp96 did not localize with lysosomes (Pearson's coefficient of colocalized volume =0.0065), suggesting that the rapid translocation of gp96 into the cytosol (Figure 7I) prevents it from being targeted to and degraded in lysosomes, also consistent with a previous report (38).

Discussion

The immune responses mediated by HSPs have been well studied for over 30 years and HSPs are currently in clinical trials. We and others have routinely tested the cross-presentation of HSP-chaperoned peptides and provision of co-stimulation by APCs *in vitro* (12–16,32,37–41). Recent observations that HSPs can prime diverse T cell and B cell responses (4,15,25–28) suggest that immune responses can be skewed by the responding APC, as shown in other settings (23). This appears to be dependent on the sum total of co-stimulation and efficiency of peptide cross-presentation by APCs. This study characterizes the APCs that are relevant for HSP-mediated immune responses. Cells that acquired gp96 predominantly express CD11c and/or CD11b in the lymph node. These populations included $CD11c^+CD11b^+$ cells which have been described as lymph node resident APCs (42,43). $CD11c^{int}$ ($CD11b^-$) cells, compatible with migratory APCs were included in the $gp96^+CD11c^+$ population. However, other markers of migratory APCs such as CD207 and $CD103^{high}$ were a minor percentage of the total $gp96^+$ population suggesting migratory APCs play a smaller role in early gp96 trafficking. Since CD207 analysis was performed at 8 hours post immunization our observations do not rule out a greater role for migratory cells in gp96 trafficking at later time points. Interestingly, distribution of gp96 in $CD11c^+$ cells changed slightly with time, increasing in $CD8^+$ cells at a later time point. However more gp96 appeared to associate with $CD11b^+$ than $CD11c^+$ cells at both time points. Several mechanisms may explain this observation and are not mutually exclusive; First, $CD11b^+$ cells are the densest population of cells along the periphery of the lymph node. These would be the first cells in contact with draining protein (44) and thus, would have preferential access to gp96 regardless of their rate of incorporation. Once gp96 begins to accumulate, $CD11c^+$ cells migrating to the edge of the lymph node may gain access. Second, gp96 may be transferred between cells through a variety of mechanisms including intercellular communication (45), CD91 dependent capture of extracellular gp96 (17), or capture of vesicle encapsulated material (46,47). Thus $CD91^+CD11b^+$ cells may transfer endocytosed gp96 to other cell types over time. Third, macrophages are known to rapidly degrade internalized material while dendritic cells do this at a slower rate (48). Extended times beyond 48 hrs may favor accumulation of gp96 in $CD11c^+$ cells. Fourth, we have not ruled out an influx of migratory cells from the periphery at later time points although changes in the total cell distribution in lymph nodes at 48 hrs were subtle. Our findings can be compared to previous studies showing an increase in $CD11c^{high}MHCII^{high}CD103^+$ APCs

NIH-PA Author Manuscript

NIH-PA Author Manuscript

NIH-PA Author Manuscript

following intraperitoneal vaccination with gp96-Ig fusion protein (22). However, since the vaccination site, draining lymph nodes, and immunizing protein (native gp96 vs gp96-Ig) are different, it was anticipated that only a partial overlap of relevant APCs subsets would be observed.

Regardless of CD11b and/or CD11c expression, the robust expression of MHC II on cells acquiring gp96 attests to the peptide presenting ability of these cells. We have successfully transferred anti-tumor immunity between mice through the adoptive transfer of $gp96^+$ cells. $Gp96^+$ cells are predominantly CD11b and CD11c expressing cells. While there may be contaminating cells not expressing these markers in the transferred population, the low numbers of total transferred cells renders these potential contaminating cells marginal. Transferred cells elicited antigen-specific tumor immunity in recipient mice only when viable suggesting that donor cells must be cross-priming competent. These conclusions are currently being confirmed in an MHC mismatched system where the recipient and/or donor APCs are unable to cross-present to recipient T cells.

Overall, we have resisted applying the nomenclature ‘macrophage’ and ‘dendritic cell’ to our $CD11b^+$ and $CD11c^+$ populations and we compare them with caution to previously characterized APC subsets (23,24,36,42,43) for the reason that there are examples of CD11b and CD11c expression on both macrophages and dendritic cells. Where appropriate, we have drawn parallels to previously characterized cell types using additional markers to clarify the phenotype of cells described in our study. Both $CD11c^+$ and $CD11b^+$ cells express some level of CD91 which satisfies one requirement for interaction with, and uptake of, HSP (13). We demonstrate that CD91 expression closely correlates with ability of APCs to endocytose gp96. $CD11c^+CD11b^+$ cells which have been characterized as lymph node resident APCs (42) express CD91 which is reflected in their superior ability to endocytose gp96. $CD11c^+CD11b^-$ cells, including $CD11c^{int}$ (or migratory APCs) express less CD91 (Supplemental Figure 4B) and are expectedly less efficient at endocytosis of gp96 than $CD11c^+CD11b^+$ cells. These results were consistent both *in vivo* and *in vitro; in vitro*, when gp96 is abundant and access to cells is not restricted, $CD11c^+CD11b^+$ APCs appear to be superior in taking up gp96. *In vivo*, gp96 would be accessible to $CD11c^+CD11b^+$ cells following diffusion of gp96 through the lymphatics, however we have not ruled out transfer of gp96 to these cells from migratory cells. Additional factors, such as retention of endocytosed material, that may contribute to the final cross-presentation event *in vivo* remain to be examined.

There is a current focus on determining how material in endosomal compartments translocates to the cytosol for processing (19,49–51). Previous studies have shown that peptides chaperoned by HSPs are processed by proteasomes and require TAP transport, prior to presentation on MHC I (13). Following endocytosis, dissociation of the peptide from gp96 occurred rapidly within a few minutes. Dissociation could reflect changes in pH or activity of compartment-specific enzymes (52). Alternatively, a recently identified endosome specific ‘unfolding’ mechanism could cause the gp96 to relinquish the chaperoned peptide (51). This ‘unfolding’ mechanism allows for stretches of polypeptides to be extruded to the cytosol. Short sequences can bypass this mechanism. Surprisingly, but consistent with this ‘unfolding’ mechanism, gp96 was observed to translocate to the cytosol rapidly and earlier than the peptide. This is also consistent with our observation that endocytosed gp96 is excluded from lysosomes. We expect that gp96 will be degraded in the cytosol (38). In addition, the delay in peptide translocation to the cytosol may explain how some of these HSP-chaperoned peptides are presented by MHC II (14). Thus, peptide-containing vesicles may fuse with MHC II loading compartments before peptide can be translocated to the cytosol. This concerted processing event and timed-translocation could explain how gp96-chaperoned peptides are presented on MHC I or MHC II by the same

NIH-PA Author Manuscript

NIH-PA Author Manuscript

NIH-PA Author Manuscript

APC. We also observed the persistence of peptide within the cytosol of cells which could be the result of re-association of peptide with endogenous HSPs within the APC (38,49,51,53,54).

The identification of physiologically relevant APCs for HSP-mediated immunity has important implications for designing vaccines to cancer and infectious disease. However, these studies also impact our understanding of effects of extracellular HSPs resulting from necrotic lysis of cells in tumor microenvironments or cell lysis associated with pathogen infection and trauma (16). Thus release of gp96 from cells and its rapid drainage to regional lymph nodes will serve to alert the immune system of cellular compromise. In the setting of immune surveillance, this mechanism may be responsible for the observed anti-tumor immunity associated with tumorigenesis. These studies identify a crucial step in priming HSP-associated immune responses.

Supplementary Material

Refer to Web version on PubMed Central for supplementary material.

Acknowledgments

We thank Dr. Jean-Charles Guéry (INSERM U563, Toulouse Cedex) for the LC21 hybridoma. We thank Nilabh Shastri (University of California, Berkley CA) for the B3Z hybridoma. We thank Drs. Kang Liu (Columbia University, NY), Adrian Morelli (University of Pittsburgh, PA) and Michael Dustin (New York University, NY) for critically reading the manuscript. RJB conceived the study. MNM, JP, LEK, SW and RJB performed the experiments. RJB and MNM wrote the manuscript.

This work was supported by NIH Grant AI079057, CA137133 and CA90440.

References

1. Srivastava PK, Udono H, Blachere NE, Li Z. Heat shock proteins transfer peptides during antigen processing and CTL priming. Immunogenetics. 1994; 39:93–98. [PubMed: 8276462]
2. Binder RJ, Srivastava PK. Essential role of CD91 in re-presentation of gp96-chaperoned peptides. Proc Natl Acad Sci USA. 2004; 101:6128–6133. [PubMed: 15073331]
3. Mo A, Musselli C, Chen H, Pappas J, Leclair K, Liu A, Chicz RM, Truneh A, Monks S, Levey DL, Srivastava PK. A heat shock protein based polyvalent vaccine targeting HSV-2: CD4(+) and CD8(+) cellular immunity and protective efficacy. Vaccine. 2011; 29:8530–8541. [PubMed: 21767588]
4. Srivastava PK, DeLeo AB, Old LJ. Tumor rejection antigens of chemically induced sarcomas of inbred mice. Proc Natl Acad Sci USA. 1986; 83:3407–3411. [PubMed: 3458189]
5. Tamura Y, Peng P, Liu K, Daou M, Srivastava PK. Immunotherapy of tumors with autologous tumor-derived heat shock protein preparations. Science. 1997; 278:117–120. [PubMed: 9311915]
6. Testori A, Richards J, Whitman E, Mann GB, Lutzky J, Camacho L, Parmiani G, Tosti G, Kirkwood JM, Hoos A, Yuh L, Gupta R, Srivastava PK. Phase III comparison of vitespen, an autologous tumor-derived heat shock protein gp96 peptide complex vaccine, with physician's choice of treatment for stage IV melanoma: the C-100–21 Study Group. J Clin Oncol. 2008; 26:955–962. [PubMed: 18281670]
7. Wood C, Srivastava P, Bukowski R, Lacombe L, Gorelov AI, Gorelov S, Mulders P, Zielinski H, Hoos A, Teofilovici F, Isakov L, Flanigan R, Figlin R, Gupta R, Escudier B. An adjuvant autologous therapeutic vaccine (HSPPC-96; vitespen) versus observation alone for patients at high risk of recurrence after nephrectomy for renal cell carcinoma: a multicentre, open-label, randomised phase III trial. Lancet. 2008; 372:145–154. [PubMed: 18602688]
8. Udono H, Srivastava PK. Heat shock protein 70-associated peptides elicit specific cancer immunity. J Exp Med. 1993; 178:1391–1396. [PubMed: 8376942]

NIH-PA Author Manuscript

NIH-PA Author Manuscript

NIH-PA Author Manuscript

9. Udono H, Srivastava PK. Comparison of tumor-specific immunogenicities of stress-induced proteins gp96, hsp90, and hsp70. J Immunol. 1994; 152:5398–5403. [PubMed: 8189059]
10. Basu S, Srivastava PK. Calreticulin, a peptide-binding chaperone of the endoplasmic reticulum, elicits tumor- and peptide-specific immunity. J Exp Med. 1999; 189:797–802. [PubMed: 10049943]
11. Wang XY, Kazim L, Repasky EA, Subjeck JR. Characterization of heat shock protein 110 and glucose-regulated protein 170 as cancer vaccines and the effect of fever-range hyperthermia on vaccine activity. J Immunol. 2001; 166:490–497. [PubMed: 11123328]
12. Binder RJ, Han DK, Srivastava PK. CD91: a receptor for heat shock protein gp96. Nat Immunol. 2000; 1:151–155. [PubMed: 11248808]
13. Basu S, Binder RJ, Ramalingam T, Srivastava PK. CD91 is a common receptor for heat shock proteins gp96, hsp90, hsp70, and calreticulin. Immunity. 2001; 14:303–313. [PubMed: 11290339]
14. Matsutake T, Sawamura T, Srivastava PK. High efficiency CD91- and LOX-1-mediated re-presentation of gp96-chaperoned peptides by MHC II molecules. Cancer Immun. 2010; 10:7. [PubMed: 20672796]
15. Pawaria S, Binder RJ. CD91-dependent programming of T-helper cell responses following heat shock protein immunization. Nat Commun. 2011; 2:521.10.1038/ncomms1524 [PubMed: 22045000]
16. Basu S, Binder RJ, Suto R, Anderson KM, Srivastava PK. Necrotic but not apoptotic cell death releases heat shock proteins, which deliver a partial maturation signal to dendritic cells and activate the NF-kappa B pathway. Int Immunol. 2001; 12:1539–1546. [PubMed: 11058573]
17. Pawaria S, Messmer MN, Zhou YJ, Binder RJ. A role for the heat shock protein-CD91 axis in the initiation of immune responses to tumors. Immunol Res. 2011; 50:255–260. [PubMed: 21717074]
18. Houlihan JL, Metzler JJ, Blum JS. HSP90alpha and HSP90beta isoforms selectively modulate MHC class II antigen presentation in B cells. J Immunol. 2009; 182:7451–7458. [PubMed: 19494268]
19. Ichiyanagi T, Imai T, Kajiwara C, Mizukami S, Nakai A, Nakayama T, Udono H. Essential role of endogenous heat shock protein 90 of dendritic cells in antigen cross-presentation. J Immunol. 2010; 185:2693–2700. [PubMed: 20668218]
20. Udono H, Levey DL, Srivastava PK. Cellular requirements for tumor-specific immunity elicited by heat shock proteins: tumor rejection antigen gp96 primes CD8+ T cells in vivo. Proc Natl Acad Sci USA. 1994; 91:3077–3081. [PubMed: 7909157]
21. Binder RJ, Anderson KM, Basu S, Srivastava PK. Cutting edge: heat shock protein gp96 induces maturation and migration of CD11c+ cells in vivo. J Immunol. 2000; 1:165:6029–6035. [PubMed: 11086034]
22. Strbo N, Pahwa S, Kolber MA, Gonzalez L, Fisher E, Podack ER. Cell-secreted Gp96-Ig-peptide complexes induce lamina propria and intraepithelial CD8+ cytotoxic T lymphocytes in the intestinal mucosa. Mucosal Immunol. 2010; 3:182–192. [PubMed: 19924120]
23. Heath WR, Belz GT, Behrens GM, Smith CM, Forehan SP, Parish IA, Davey GM, Wilson NS, Carbone FR, Villadangos JA, Heath WR, Belz GT, Behrens GMN, Smith CM, Forehan SP, Parish IA, Davey GM, Wilson NS, Carbone FR, Villadangos JA. Cross-presentation, dendritic cell subsets, and the generation of immunity to cellular antigens. Immunological Reviews. 2004; 199:9–26. [PubMed: 15233723]
24. Liu K, Nussenzweig MC. Origin and development of dendritic cells. Immunol Rev. 2010; 234:45–54. [PubMed: 20193011]
25. Wang S, Qiu L, Liu G, Li Y, Zhang X, Jin W, Gao GF, Kong X, Meng S. Heat shock protein gp96 enhances humoral and T cell responses, decreases Treg frequency and potentiates the anti-HBV activity in BALB/c and transgenic mice. Vaccine. 2011; 29:6342–6351. [PubMed: 21600951]
26. Navaratnam M, Deshpande MS, Hariharan MJ, Zatechka DS Jr, Srikumaran S. Heat shock protein-peptide complexes elicit cytotoxic T-lymphocyte and antibody responses specific for bovine herpesvirus 1. Vaccine. 2001; 19:1425–1434. [PubMed: 11163665]
27. Chandawarkar RY, Wagh MS, Srivastava PK. The dual nature of specific immunological activity of tumor-derived gp96 preparations. J Exp Med. 1999; 189:1437–1442. [PubMed: 10224283]

NIH-PA Author Manuscript

NIH-PA Author Manuscript

NIH-PA Author Manuscript

28. Chandawarkar RY, Wagh MS, Kovalchin JT, Srivastava PK. Immune modulation with high-dose heat-shock protein gp96: therapy of murine autoimmune diabetes and encephalomyelitis. Int Immunol. 2004; 16:615–624. [PubMed: 15039392]
29. Blachere NE, Li Z, Chandawarkar RY, Suto R, Jaikaria NS, Basu S, Udono H, Srivastava PK. Heat shock protein-peptide complexes, reconstituted in vitro, elicit peptide-specific cytotoxic T lymphocyte response and tumor immunity. J Exp Med. 1997; 186:1315–1322. [PubMed: 9334371]
30. Shastri N, Gonzalez F. Endogenous generation and presentation of the ovalbumin peptide/Kb complex to T cells. J Immunol. 1993; 150:2724–2736. [PubMed: 8454852]
31. Wei BY, Gervois N, Mer G, Adorini L, Benoist C, Mathis D. Exogenous peptides compete for the presentation of endogenous antigens to major histocompatibility complex class II-restricted T cells. J Exp Med. 1991; 174:945–948. [PubMed: 1919443]
32. Binder RJ, Harris ML, Ménoret A, Srivastava PK. Saturation, competition, and specificity in interaction of heat shock proteins (hsp) gp96, hsp90, and hsp70 with CD11b+ cells. J Immunol. 2000; 165:2582–2587. [PubMed: 10946285]
33. Hanson HL, Donermeyer DL, Ikeda H, White JM, Shankaran V, Old LJ, Shiku H, Schreiber RD, Allen PM. Eradication of established tumors by CD8+ T cell adoptive immunotherapy. Immunity. 2000; 13:265–276. [PubMed: 10981969]
34. Banerjee PP, Vinay DS, Mathew A, Raje M, Parekh V, Prasad DV, Kumar A, Mitra D, Mishra GC. Evidence that glycoprotein 96 (B2), a stress protein, functions as a Th2-specific costimulatory molecule. J Immunol. 2002; 169:3507–3518. [PubMed: 12244140]
35. Eriksson C, Rantapää-Dahlqvist S, Sundqvist KG. T-cell expression of CD91 - a marker of unresponsiveness to anti-TNF therapy in rheumatoid arthritis. APMIS. 2010; 118:837–845. [PubMed: 20955456]
36. Lutz MB, Kukutsch N, Ogilvie AL, Rossner S, Koch F, Romani N, Schuler G. An advanced culture method for generating large quantities of highly pure dendritic cells from mouse bone marrow. J Immunol Methods. 1999; 223:77–92. [PubMed: 10037236]
37. Singh-Jasuja H, Toes RE, Spee P, Munz C, Hilf N, Schoenberger SP, Ricciardi-Castagnoli P, Neefjes J, Rammensee HG, Arnold-Schild D, Schild H. Cross-presentation of glycoprotein 96-associated antigens on major histocompatibility complex class I molecules requires receptor-mediated endocytosis. J Exp Med. 2000; 191:1965–1974. [PubMed: 10839811]
38. Binder RJ, Blachere NE, Srivastava PK. Heat shock protein-chaperoned peptides but not free peptides introduced into the cytosol are presented efficiently by major histocompatibility complex I molecules. J Biol Chem. 2001; 276:17163–17171. [PubMed: 11278929]
39. Noessner E, Gastpar R, Milani V, Brandl A, Hutzler PJ, Kuppner MC, Roos M, Kremmer E, Asea A, Calderwood SK, Issels RD. Tumor-derived heat shock protein 70 peptide complexes are cross-presented by human dendritic cells. J Immunol. 2002; 169:5424–5432. [PubMed: 12421917]
40. Tobian AA, Canaday DH, Boom WH, Harding CV. Bacterial heat shock proteins promote CD91-dependent class I MHC cross-presentation of chaperoned peptide to CD8+ T cells by cytosolic mechanisms in dendritic cells versus vacuolar mechanisms in macrophages. J Immunol. 2004; 172:5277–5286. [PubMed: 15100266]
41. Robert J, Ramanayake T, Maniero GD, Morales H, Chida AS. Phylogenetic conservation of glycoprotein 96 ability to interact with CD91 and facilitate antigen cross-presentation. J Immunol. 2008; 180:3176–3182. [PubMed: 18292541]
42. Villadangos JA, Heath WR. Life cycle, migration and antigen presenting functions of spleen and lymph node dendritic cells: limitations of the Langerhans cells paradigm. Semin Immunol. 2005; 17:262–272. [PubMed: 15946854]
43. Romani N, Clausen BE, Stoitzner P. Langerhans cells and more: langerin-expressing dendritic cell subsets in the skin. Immunol Rev. 2010; 234:120–141. [PubMed: 20193016]
44. Gray EE, Cyster JG. Lymph node macrophages. J Innate Immun. 2012; 4:424–436. [PubMed: 22488251]
45. Watkins SC, Salter RD. Functional connectivity between immune cells mediated by tunneling nanotubules. Immunity. 2005; 23:309–318. [PubMed: 16169503]
46. Blachère NE, Darnell RB, Albert ML. Apoptotic cells deliver processed antigen to dendritic cells for cross-presentation. PLoS Biol. 2005; 3:e185. [PubMed: 15839733]

NIH-PA Author Manuscript

NIH-PA Author Manuscript

NIH-PA Author Manuscript

47. Asano K, Nabeyama A, Miyake Y, Qiu CH, Kurita A, Tomura M, Kanagawa O, Fujii S, Tanaka M. CD169-positive macrophages dominate antitumor immunity by crosspresenting dead cell-associated antigens. Immunity. 2011; 34:85–95. [PubMed: 21194983]

48. Delamarre L, Pack M, Chang H, Mellman I, Trombetta ES. Differential lysosomal proteolysis in antigen-presenting cells determines antigen fate. Science. 2005; 307:1630–1634. [PubMed: 15761154]

49. Oura J, Tamura Y, Kamiguchi K, Kutomi G, Sahara H, Torigoe T, Himi T, Sato N. Extracellular heat shock protein 90 plays a role in translocating chaperoned antigen from endosome to proteasome for generating antigenic peptide to be cross-presented by dendritic cells. Int Immunol. 2011; 23:223–237. [PubMed: 21421737]

50. Imai T, Kato Y, Kajiwara C, Mizukami S, Ishige I, Ichiyanagi T, Hikida M, Wang JY, Udono H. Heat shock protein 90 (HSP90) contributes to cytosolic translocation of extracellular antigen for cross-presentation by dendritic cells. Proc Natl Acad Sci U S A. 2011; 108:16363–16368. [PubMed: 21930907]

51. Kato Y, Kajiwara C, Ishige I, Mizukami S, Yamazaki C, Eikawa S, Kakimi K, Udono H. HSP70 and HSP90 Differentially Regulate Translocation of Extracellular Antigen to the Cytosol for Cross-Presentation. Autoimmune Dis. 2012; 2012:745962. [PubMed: 23050124]

52. Watts C. Capture and processing of exogenous antigens for presentation on MHC molecules. Annu Rev Immunol. 1997; 15:821–850. [PubMed: 9143708]

53. Ishii T, Udono H, Yamano T, Ohta H, Uenaka A, Ono T, Hizuta A, Tanaka N, Srivastava PK, Nakayama E. Isolation of MHC class I-restricted tumor antigen peptide and its precursors associated with heat shock proteins hsp70, hsp90, and gp96. J Immunol. 1999; 162:1303–1309. [PubMed: 9973383]

54. Li C, Buckwalter MR, Basu S, Garg M, Chang J, Srivastava PK. Dendritic cells sequester antigenic epitopes for prolonged periods in the absence of antigen-encoding genetic information. Proc Natl Acad Sci USA. 2012; 109:17543–17548. [PubMed: 23045695]

NIH-PA Author Manuscript
NIH-PA Author Manuscript
NIH-PA Author Manuscript

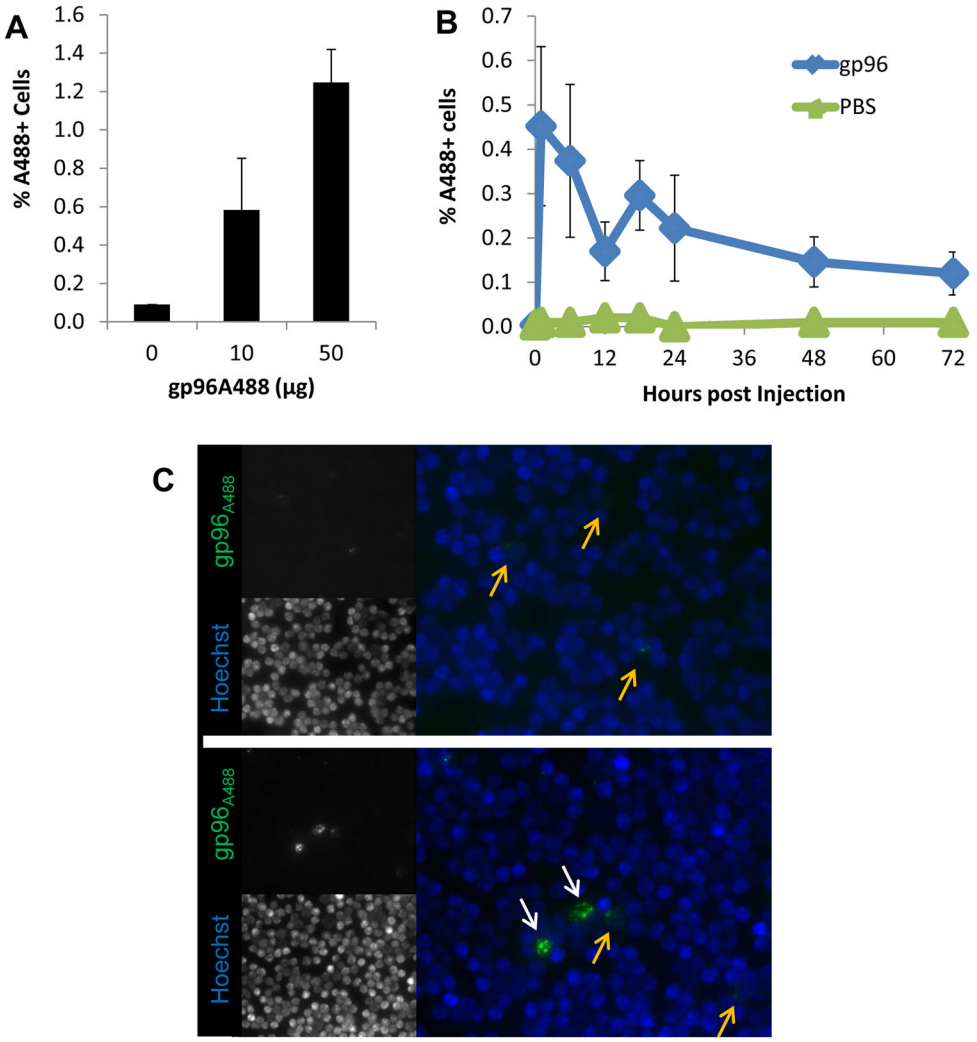

Figure 1. Rapid localization of gp96 in lymph nodes following intradermal immunization

(A) C57BL/6 mice were treated with titrated doses of $gp96_{A488}$ intradermally. Draining lymph nodes were harvested 8 hours later and analyzed by flow cytometry. Results shown are averaged from 3 independent experiments, of 4–8 mice per group. (B) Lymph nodes from mice receiving 10 μg $gp96_{A488}$ were harvested at the indicated time points and analyzed as above. Data are representative of three experiments, of 5 mice per time point for gp96 group and 2 per time point for PBS. (C) Lymph nodes from mice receiving 10 μg $gp96_{A488}$ were harvested at 5 hours, disrupted into single cell suspensions and analyzed by microscopy. Nuclei were stained with Hoechst dye (blue), A488 is shown in green. Two images at 40x magnification are shown to demonstrate cells with low (yellow arrows) and high (white arrows) $gp96_{A488}$ staining. Data (A, B) are represented as mean +/− SEM.

NIH-PA Author Manuscript
NIH-PA Author Manuscript
NIH-PA Author Manuscript

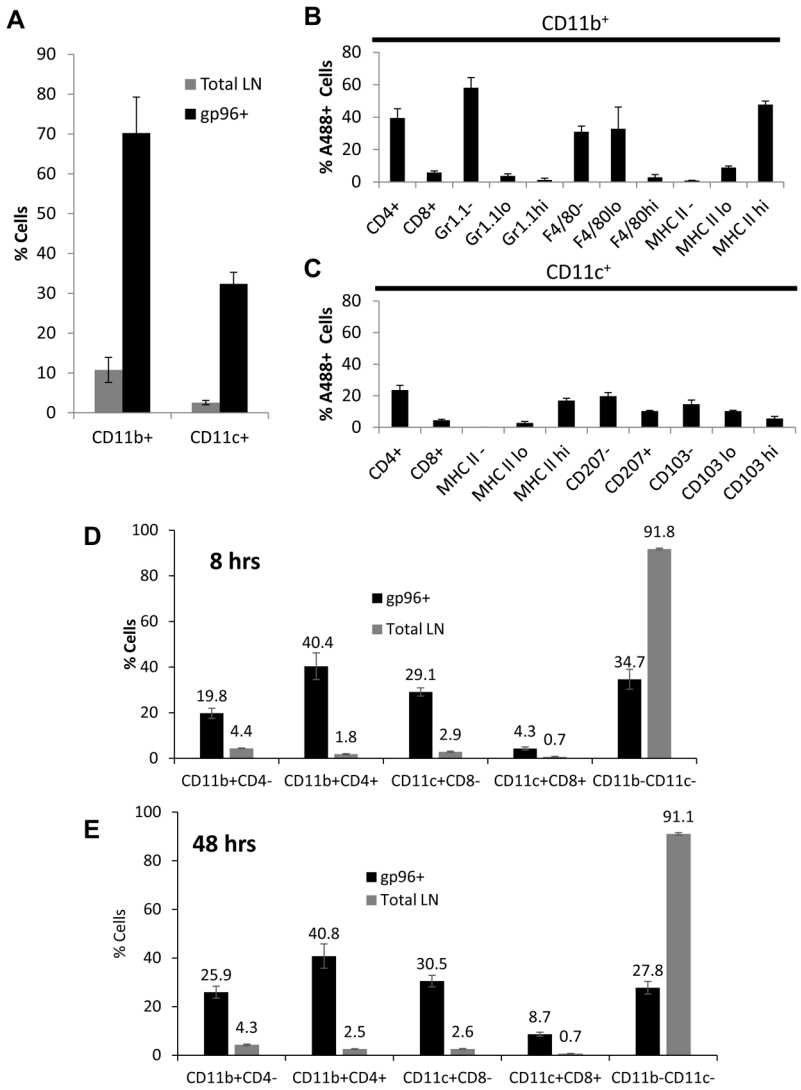

Figure 2. Phenotypic analysis of lymph node cells associated with gp96$_{A488}$

Lymph nodes from unimmunized or gp96 immunized mice were analyzed by multi-color flow cytometry. (A) At 8 hours post immunization with 10 μg gp96$_{A488}$, total lymph node and gp96+ cells were phenotyped for CD11c and CD11b expression. The CD11c population was CD11b$^{+/-}$ and CD11b^{+} population was CD11c$^{+/-}$. (B) A488^{+}CD11b^{+} lymph node cells were additionally phenotyped for CD4, CD8, Gr1.1, F4/80 and MHC II. (C) A488^{+}CD11c^{+} lymph node cells were additionally phenotyped for CD4, CD8, CD207, CD103 and MHC II. At 8 (D) or 48 (E) hours post immunization with 10 μg gp96$_{A488}$, lymph nodes were harvested and phenotyped for the indicated populations. The distribution of gp96 in each population is indicated as a percentage and compared to the percentage of that population in the total lymph node. Percentages are the average from 5 mice, and representative of 2 experiments. Data are represented as mean +/− SEM.

NIH-PA Author Manuscript
NIH-PA Author Manuscript
NIH-PA Author Manuscript

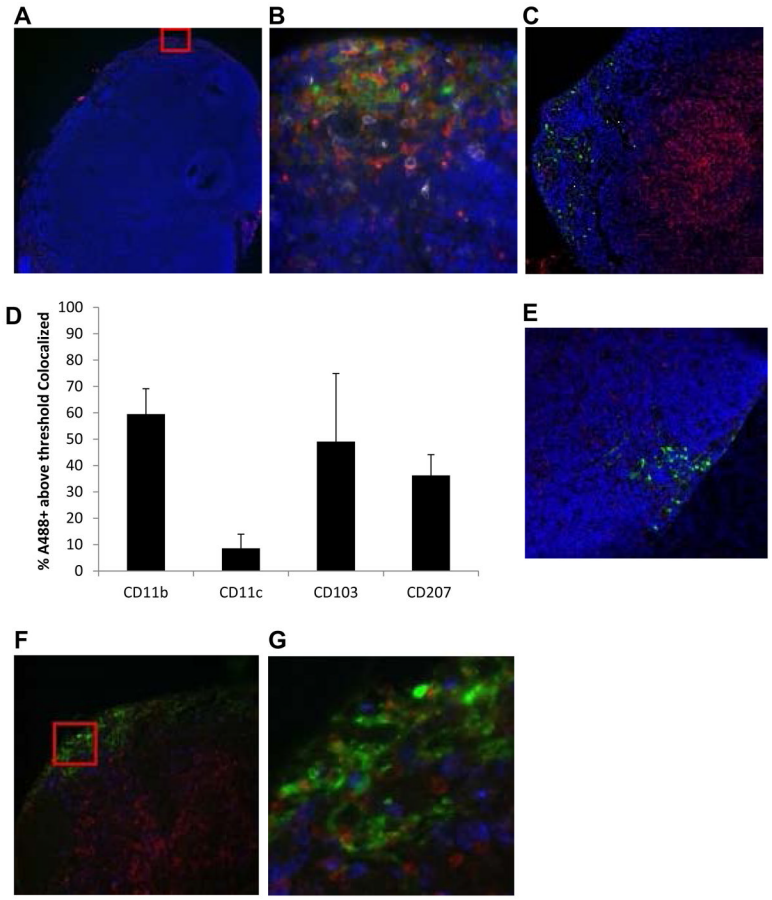

Figure 3. Distribution of gp96$_{A488}^{+}$ cells within the lymph node

Mice were immunized with 10 μg gp96$_{A488}$ and draining lymph nodes were harvested 8 hours later and analyzed by fluorescent microscopy. Green indicates gp96$_{A488}$ fluorescence and blue is Hoechst nuclear staining. (A) Images captured at 10x magnification. Region of Interest (ROI, red box) was selected for further analysis. (B) ROI is analyzed for CD11b (red) and CD11c (white). (C) Image at 20x magnification showing CD8 stain to reveal T cell zones. (D) Images were analyzed using IMARIS and the co-localization of each marker indicated with gp96$_{A488}$ was quantified and expressed as percent A488^{+} above threshold that co-localized. Each marker (red or white) was analyzed separately and there is potential overlap with other indicated markers. Data are the average value from 3 ROIs analyzed. Data are represented as mean +/− SEM. (E) Sections at 20x magnification were stained for CD207. Co-localization of CD207 with gp96$_{A488}$ was quantified (D). (F) Sections at 40x magnification were stained for CD103 (red). (G) ROI from (F) showing co-localization of CD103 (red) with gp96$_{A488}$ (green). Co-localization was quantified (D). Images and calculations are representative of 2 independent experiments.

NIH-PA Author Manuscript
NIH-PA Author Manuscript
NIH-PA Author Manuscript

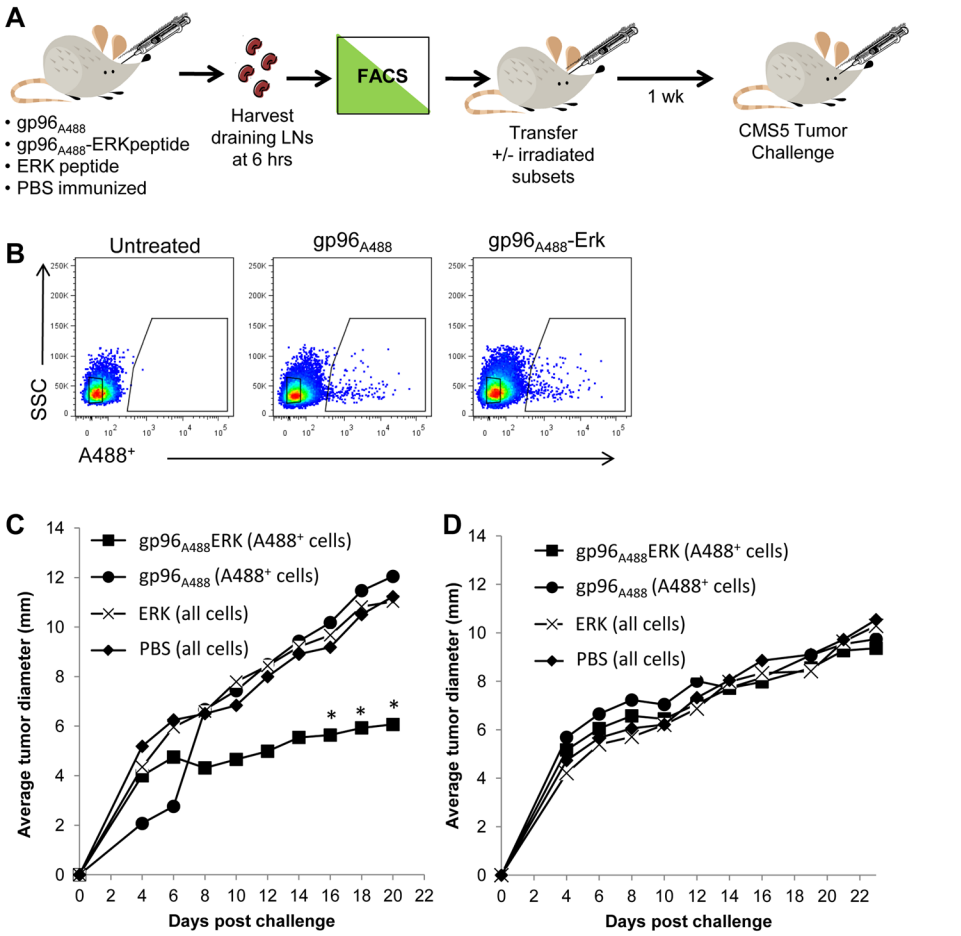

Figure 4. Adoptive transfer of tumor immunity by $gp96_{A488}^{+}$ lymph node cells

(A) A schematic of adoptive transfer of tumor immunity. Groups of mice were immunized with $gp96_{A488}$-ERK or $gp96_{A488}$. Draining lymph nodes were harvested 6 hours later. $Gp96_{A488}^{+}$ cells were purified by FACS and transferred to naïve mice. Whole lymph node cells from mice immunized with ERK alone or PBS were transferred into other naïve mice. Recipient mice were challenged with CMS5 tumor 1 week later. Tumor growth was monitored. (B) Representative FACS plots showing gated cells that were transferred. (C) CMS5 growth curves in recipient mice following transfer of donor cells. Average values calculated from 2–8 recipient mice from 2 independent experiments. *$p < 0.05$, compared to $gp96_{A488}$ recipients. (D) CMS5 growth curves in recipient mice following transfer of irradiated donor cells. Average values are from 2–5 recipient mice per group.

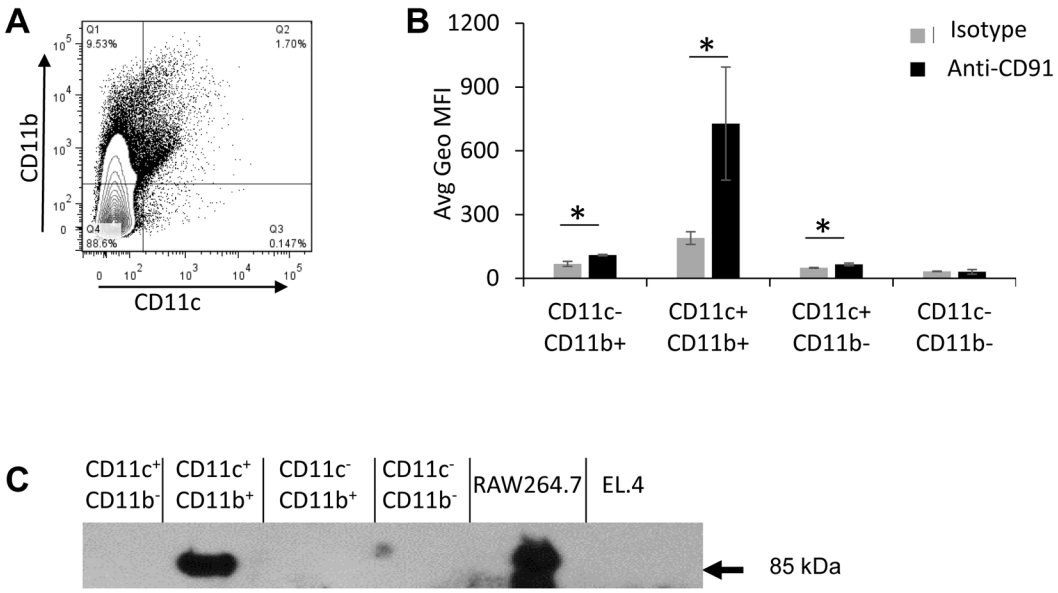

Figure 5. Expression of CD91 on subsets of APCs in the lymph node. Lymph node cells were analyzed by multi-color flow cytometry for CD11b, CD11c, and CD91. (A) Cells were first gated on CD11b and CD11c subsets, and then the average geometric mean fluorescence intensity for CD91 was quantified for each population and compared to secondary alone (B). Data are averages for three mice +/− SEM, and representative of 3 experiments. (C) CD91 expression on CD11c/CD11b populations was confirmed by FACS sorting followed by SDS-PAGE and immunoblotting. CD91 β-chain (85kDa) is identified by the arrow. Positive and negative control cell lines for CD91 were RAW264.7 and EL.4 respectively.

NIH-PA Author Manuscript NIH-PA Author Manuscript NIH-PA Author Manuscript

NIH-PA Author Manuscript
NIH-PA Author Manuscript
NIH-PA Author Manuscript

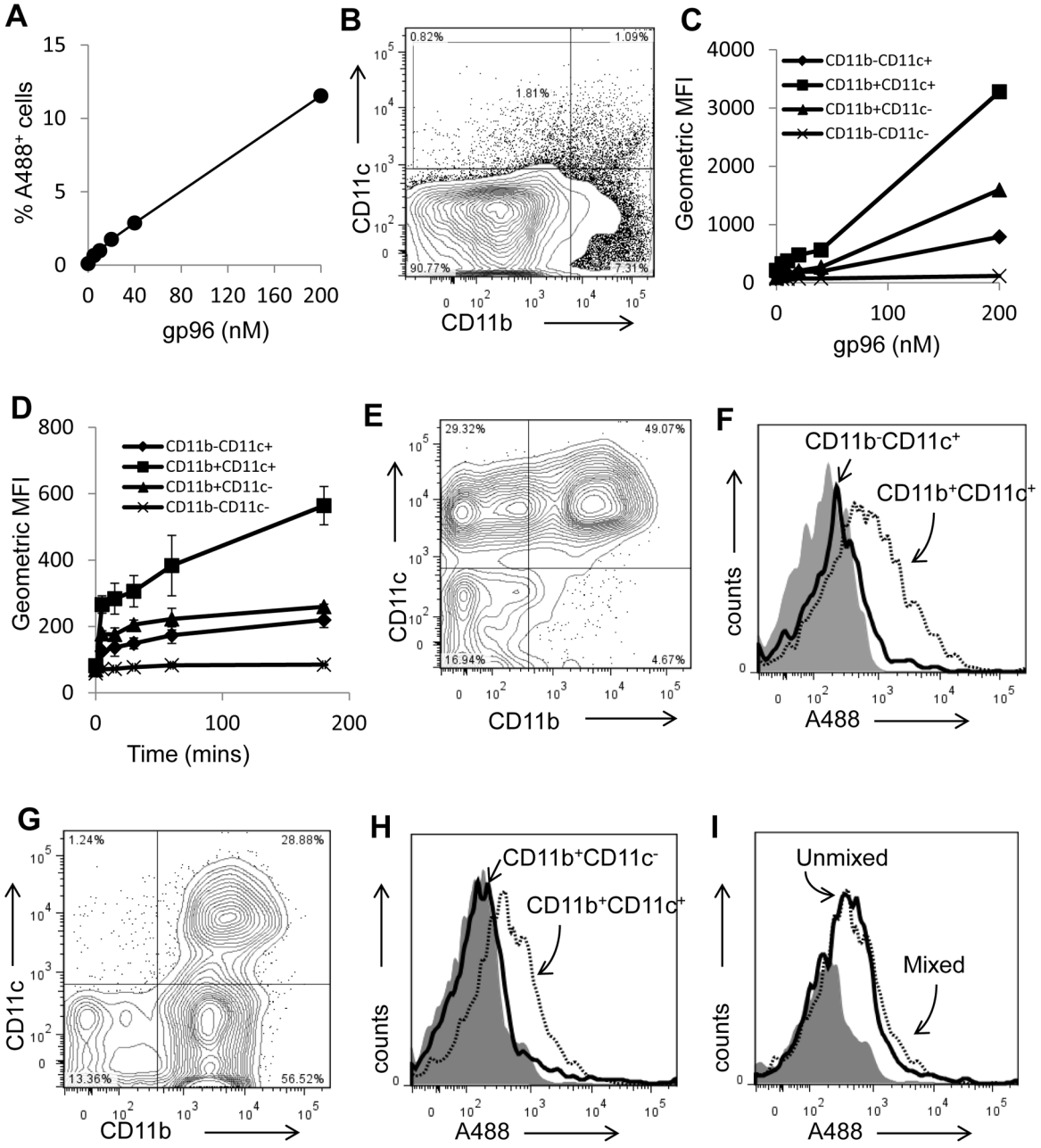

Figure 6. Differential capacities of APC subsets to endocytose gp96

(A) Isolated lymph node cells were incubated with titrated doses of $gp96_{A488}$. Cells were analyzed by flow cytometry for A488 positivity and expressed as a percentage of the total population. (B) The lymph node cells were gated into populations expressing $CD11c^+$ and/or $CD11b^+$. (C) Following incubation of lymph node cells with varying doses of $gp96_{A488}$, these populations were analyzed for endocytosis of $gp96_{A488}$. Experiments were performed in duplicates. (D) Endocytosis of $gp96_{A488}$ by the indicated populations was tested by incubating lymph node cells with 20 nM $gp96_{A488}$ for the indicated time. Experiments were performed in duplicates. (E) Competitive endocytosis was examined by mixing purified populations of $CD11b^-CD11c^+$ and $CD11b^+CD11c^+$ cells with sub-saturation amount of $gp96_{A488}$. A representative FACS plot of the cell mixture is shown. (F) An analyses of the

NIH-PA Author Manuscript

NIH-PA Author Manuscript

NIH-PA Author Manuscript

two populations of cells from (E), for A488 positivity are presented as histograms. (G) Competitive endocytosis was examined by mixing purified populations of $CD11b^{+}CD11c^{-}$ and $CD11b^{+}CD11c^{+}$ cells in the presence of sub-saturation amount of $gp96_{A488}$ cells. A representative FACS plot of the cell mixture is shown. (H) An analysis of the two populations of cells from (G), for A488 positivity are presented as histograms. (I) The endocytosis of sub-saturating amounts of $gp96_{A488}$ by $CD11b^{+}CD11c^{+}$ cells, in the presence or absence of $CD11b^{+}$ cells, is shown. Data (A, C, D) are represented as mean +/− SEM.

NIH-PA Author Manuscript

NIH-PA Author Manuscript

NIH-PA Author Manuscript

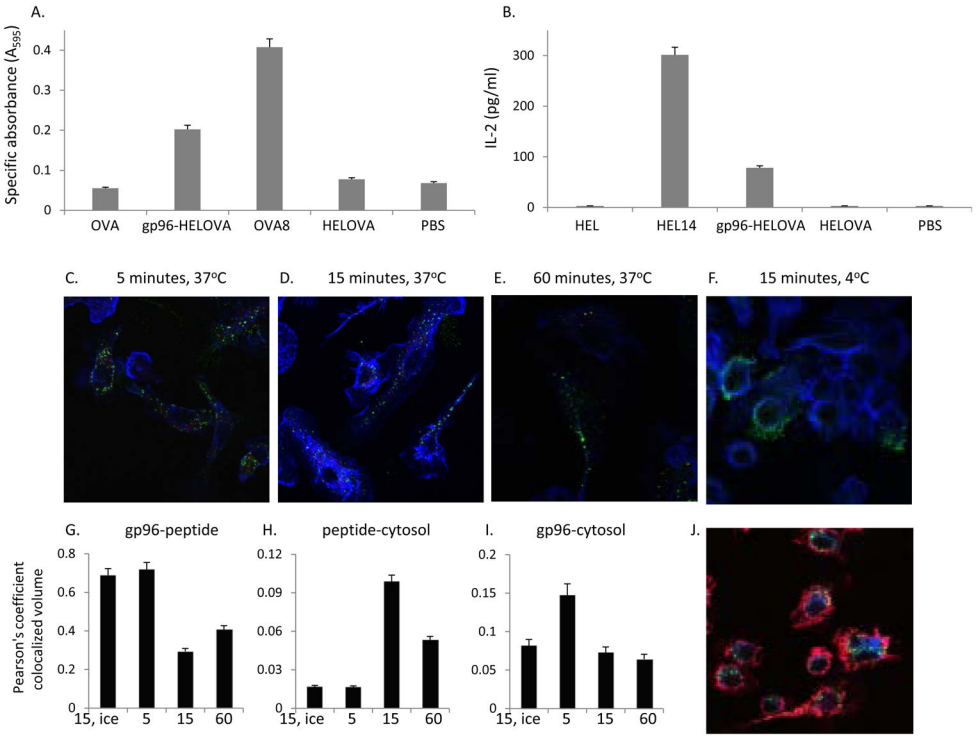

Figure 7. Cross-presentation of HSP-chaperoned peptides by CD11b^{+}CD11c^{+} BMDCs

(A) Cross presentation of HSP-chaperoned peptides by MHC I of CD11b^{+}CD11c^{+} cells was tested by incubation of cells with gp96-HELOVA. Response by B3Z was measured as specific absorbance at 595nm. Controls include cells with HELOVA alone, OVA, ova 8mer peptide and PBS. (B) Cross presentation of HSP-chaperoned peptides by MHC II of CD11b^{+}CD11c^{+} cells was tested by incubation of cells with gp96-HELOVA. Response by LC21 was measured by ELISA for IL-2. Controls include incubations of cells with HELOVA alone, HEL, HEL14 mer peptide and PBS. (C–F) gp96$_{A488}$-b-pep20 was incubated with CD11b^{+}CD11c^{+} cells on cover slips at 37°C (C–E) or 4°C (F), for the indicated time points and then stained with strepavidin-Cy3 for the peptide (red) and phalloidin (blue). Gp96$_{A488}$ appears as a green signal. (G–I) Images were analyzed using IMARIS and co-localization of gp96$_{A488}$ with peptide (G), peptide with the phalloidin (H), or gp96 with the phalloidin (I) was quantified. (J) gp96$_{A488}$ was incubated with CD11b^{+}CD11c^{+} cells on cover slips for 15 mins after which cells were fixed and stained for LAMP-1 (blue) and phalloidin (red). Co-localization of gp96$_{A488}$ with LAMP-1 was quantified by IMARIS. Experiments in (A) and (B) are representative of 3 independent experiments. Experiments in (C–J) are representative images from numerous independent experiments. Error bars are standard deviation of duplicates (A and B) and multiple ROIs in (G–I). Data (A, B G–I) are represented as mean +/− SEM.